JOURNAL OF MATERIALS SCIENCE 10 (1975) 983–997

Tensile and creep strengths of hot-pressed Si_3N_4

RAM KOSSOWSKY, D. G. MILLER, E. S. DIAZ
Materials Science Section, Metallurgy and Metals Processing Department, Westinghouse Research Laboratories, Pittsburgh, Pennsylvania, USA

Tensile, creep, and stress-rupture data for Norton HS-110 and HS-130 hot-pressed Si_3N_4 are presented. It is shown that the strength of the material is controlled by the grain-boundary glass phase. At elevated temperatures, $> 1000°C$, deformation is controlled by grain-boundary sliding. A model based on the concept of geometrically necessary wedge cracks is then developed which accounts for the observed effects of strain rate, stress, temperature, environment, and impurity content. It is concluded that the currently available hot-pressed Si_3N_4 is creep strain limited.

1. Introduction

The potential of silicon nitride (Si_3N_4) as a structural material for high temperature gas turbine applications was recognized in the early fifties. A broad study of the mechanical behaviour of Si_3N_4 at temperatures to 1200 °C was reported by Glenny and Taylor [1]. These studies which were performed on three grades of reaction sintered material and two grades of hot-pressed material included mechanical strength, bend creep, and thermal fatigue.

Interest in silicon nitride was renewed when high density, high strength grades of hot-pressed material were developed. A government program funded by the Advanced Research Projects Agency (ARPA) to design and evaluate ceramics in gas turbines led to a focused effort to establish the engineering properties of hot-pressed Si_3N_4. Tensile strength, creep strength, and stress rupture characteristics are among the properties that define the applicability of the material as structural components of the gas turbine.

This paper reports on the tensile and creep strength of Norton HS-110 and HS-130 hot-pressed Si_3N_4 as determined under the ARPA program [2]. These properties are discussed with reference to the microstructural characteristics of the material. A model for the observed behaviour is proposed and ways to improve the material performance are suggested.

2. Experimental

2.1. Material

Material was obtained from the Norton Company in the form of hot-pressed billets, 15 cm × 15 cm × 2.5 cm. Two grades of material were studied: HS-110* and HS-130. The major difference between the two grades is in the level of a few impurities [3]. HS-110 contains about 1 wt % Al and 0.5 wt % Ca as compared to 0.1 Al and 0.04 Ca in HS-130. Richerson and others [4-6] have recognized that the high temperature strength of Si_3N_4 is very sensitive to the level of alkaline† impurities, in particular Ca. Because of this, billets and specimens machined from them were classified into four groups based upon chemical composition as shown in Table I. Data reported here serve to justify this somewhat arbitrary classification. The methods of analysis are discussed elsewhere [3].

2.2. Specimens and test methods

Specimen preparation and testing procedures were described in detail previously [6]. Briefly stated, however, the typical tensile specimen had a uniform gauge length of 38.1 mm and a gauges diameter of 6.2 mm while that used to measure elastic modulus, specifically, was larger, with a 57.2 mm gauge length and 6.2 mm gauge diameter.

Elastic modulus was determined from uniaxial tensile tests.‡ Strain at low temperatures,

*HS-110 grade has been discontinued by Norton.
†We will refer to alkaline metal, Li, K, Na and the alkaline earth metal Ca, as "alkaline impurities".
‡Temperatures were recorded in °F. Loads and elongations were measured in lb and inches, respectively.

TABLE I Chemistry of Si_3N_4 billets (wt %)

Group designation	Ca	Na	K	Al	Fe	Mg
HS-110A	0.5	0.002–0.004	0.002–0.004	0.5–1.0	1.0	0.5
HS-110B	0.1–0.2	0.004–0.005	0.004–0.008	0.1	1.0	0.5
HS-130A	0.06–0.08	0.006–0.01	0.004–0.008	0.1–0.2	0.5	0.3–0.4
HS-130B	0.03–0.05	0.004–0.006	0.004–0.006	0.2–	0.5	0.3–0.4

$< 200\,^{\circ}C$, was measured by three strain gauges positioned at 120° intervals around the gauge section of the specimen. These gauges were used initially to align each specimen within 3% bend strain. At temperatures above 200°C strain was measured by an extensometer attached to the specimen activating a LVDT measuring device outside the furnace. It was possible to calculate Poisson's ratio from diametral strain as measured by two strain gauges wrapped around the specimen at opposite ends of the gauge section.

The tensile creep specimens were identical to the short tensile specimens, i.e. 6.2 mm gauge diameter and 38.1 mm gauge length. Creep tests were conducted in helium using molybdenum or graphite grips and in air using TD nickel-chrome grips. Standard dead load machines were employed with strain measured from the total load strain outside the furnace. When total creep strains read from the curves were compared with those measured by reassembling the two halves of the broken specimens, the agreement was always within 10%.§

Specimens for measuring shear modulus and strength were made with square ends to accommodate the gripping arrangement in the torsion machine. The gauge length and gauge diameter were 44.5 mm and 6.2 mm, respectively. Twist angles were measured from point indicators attached at both ends of the gauge section.

Microstructural details of tested specimens were investigated by light microscopy, scanning electron microscopy and replica and thin foil transmission electron microscopy. Details of specimen preparation and observation techniques are given elsewhere [3, 7].

3. Results

3.1. Test results

Typical tensile and torsion stress-strain curves

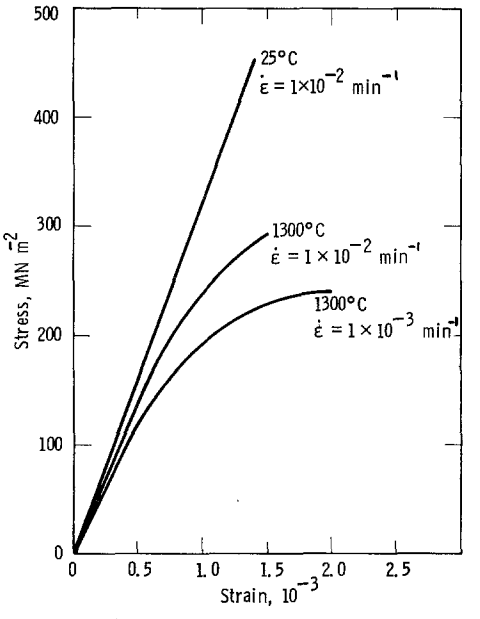

Figure 1 Typical tensile stress strain curves HS 130A.

are shown in Figs. 1 and 2, respectively. Lower strain rates produce lower strengths and higher strains to failure. The effect is pronounced in the torsional test data. However, scatter in the data appears to mask the strain-rate sensitivity when tensile results from many tests are plotted with respect to temperature in Fig. 3.

The elastic and shear modulii are plotted as functions of temperature in Fig. 4. A rate effect is observed again in the modulus of elasticity, when the results of sonic resonance measurements [8] are compared with data derived from uniaxial tensile tests. While there is little or no difference at low temperature, the strain rate affects the high temperature results significantly.

Poisson's ratio (ν) was calculated from the

§Preliminary creep tests at comparable loads have also been conducted on SiC specimens. No appreciable creep strains were measured indicating that neither the load train nor grips, *per se*, contributed to measured strain as presented here.

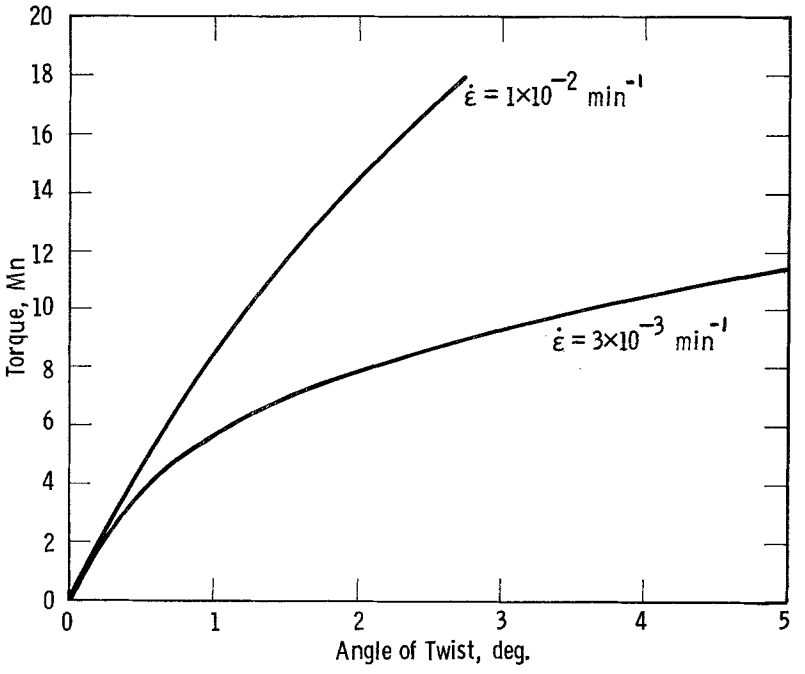

Figure 2 Shear test curves in air, 1260°C HS 130A.

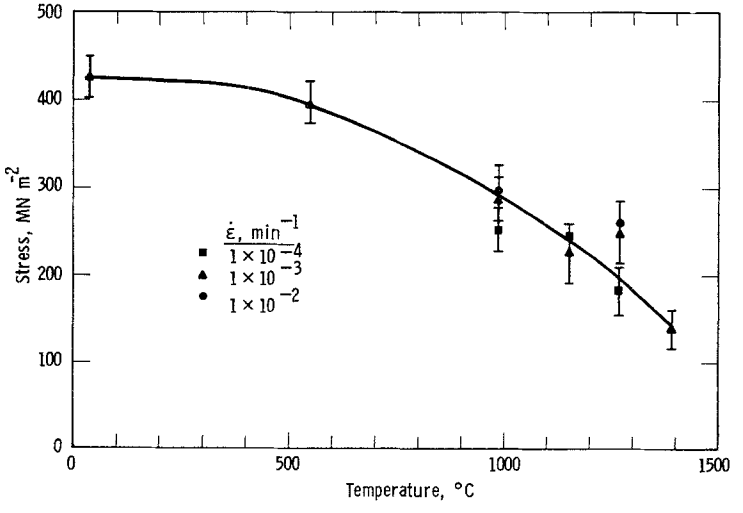

Figure 3 Tensile strength of hot-pressed Si_3N_4. Points are average of data; bars indicate standard deviation.

elastic (E) and the shear modulii (G) using the expression:

$$G = \frac{E}{2(1 + \nu)} \cdot \quad (1)$$

The value of 0.28 at 25°C is in very good agreement with the measured value for ν of 0.27 and Poisson's ratio does not appear to change with temperature. However, for elevated temperatures, Poisson's ratio must be calculated from high rate data to avoid the effect of plastic relaxation. Unfortunately, data for G at ultrasonic rates are not available.

Typical creep results are shown in Fig. 5. The general shape of the strain-time curve is similar to that considered characteristic of most metals. There is a first or transition stage where the strain rate decreases rather rapidly with time. This is followed by steady state creep or stage two which extends over most of the life span of

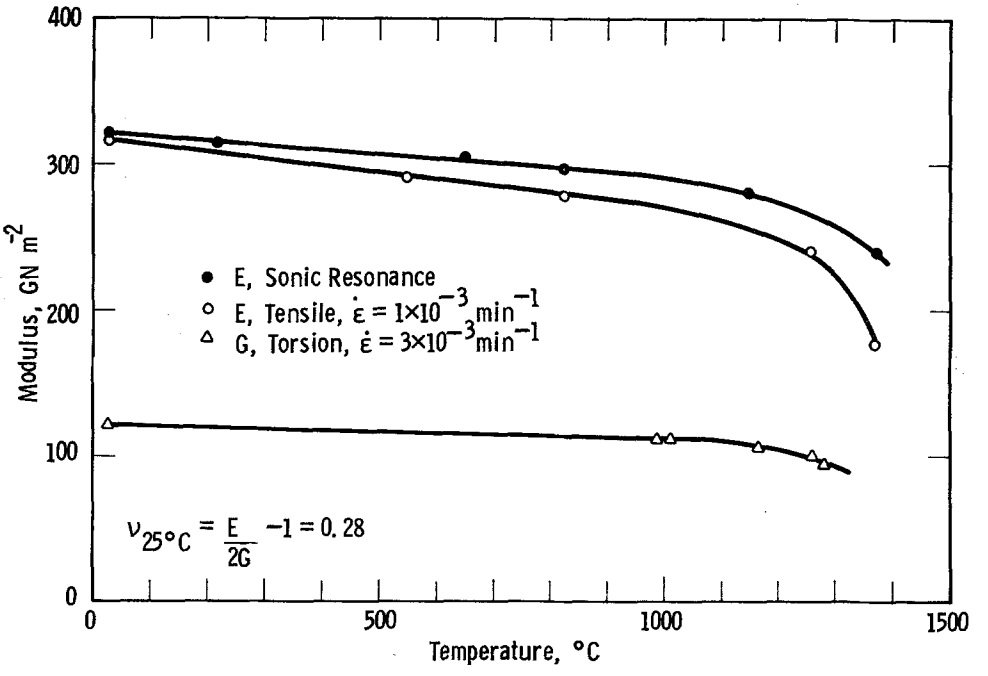

Figure 4 Elastic and shear modulii as a function of temperature in air.

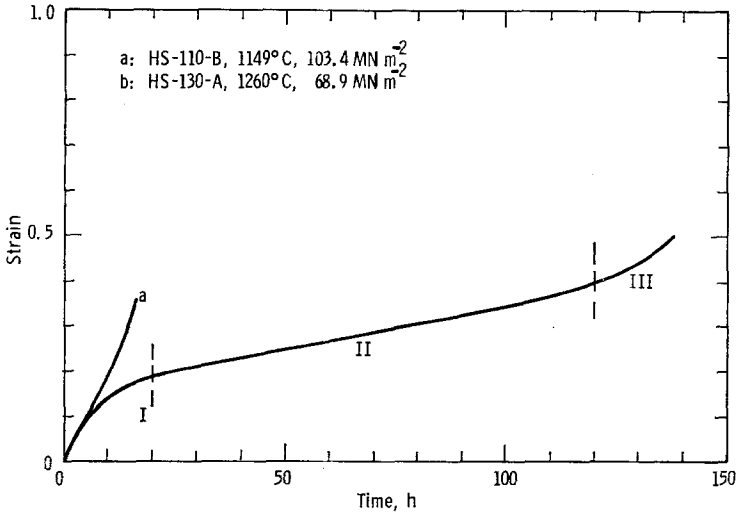

Figure 5 Strain-time curves, hot-pressed Si_3N_4, creep tests in He.

the specimen. The third stage or stage of accelerated creep is rather short and in many cases not detected at all. Steady state creep may be absent under certain conditions of temperature, stress, or material impurity. In such instances, accelerated creep will commence almost immediately resulting in an abbreviated life time at very low creep strain. Figs. 6 and 7 illustrate the effects of stress, temperature, purity, and environment on stress-rupture life and time to reach 1% plastic strain, respectively. A substantial increase in life is observed for tests in air over tests in He for materials of comparable purity. A small decrease in the

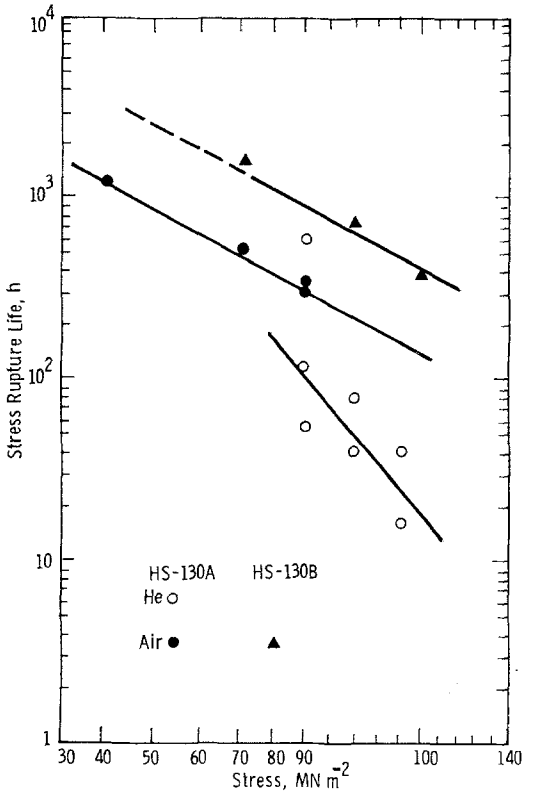

Figure 6 Stress rupture, hot-pressed Si_3N_4 at 1260°C.

level of alkaline impurities results in a significant increase in stress rupture life. Similarly, the time to reach 1% strain increases with purity and decreases with increasing temperature. Furthermore, the data from Table II indicate that life in a helium atmosphere is shorter than life in air and that failure occurs at less than 1% total strain in helium in contrast to 3% total strain in air.

The relationship between steady state creep rate and stress is expressed as

$$\dot{\epsilon}_s = A(\sigma,T,S,e)\sigma^n \exp\left[-\frac{\Delta H_c,\sigma,T,S,e}{RT}\right] \qquad (2)$$

where the pre-exponential term, A, and the activation enthalpy for creep, ΔH_c, are functions of stress, temperature, structure, and environment. The structural term, S, may include such parameters as grain size, dislocation density, and purity. There were no variations in grain size or dislocation structure among all the specimens tested [3]. However, the data in Figs. 6 and 7 and in Table II show that purity and test environment affect the creep properties of Si_3N_4.

Graphs of log $\dot{\epsilon}_s$ versus $1/T$ and log $\dot{\epsilon}_s$ versus σ were prepared to separate the other variables in Equation 2. In Fig. 8, for example, steady state

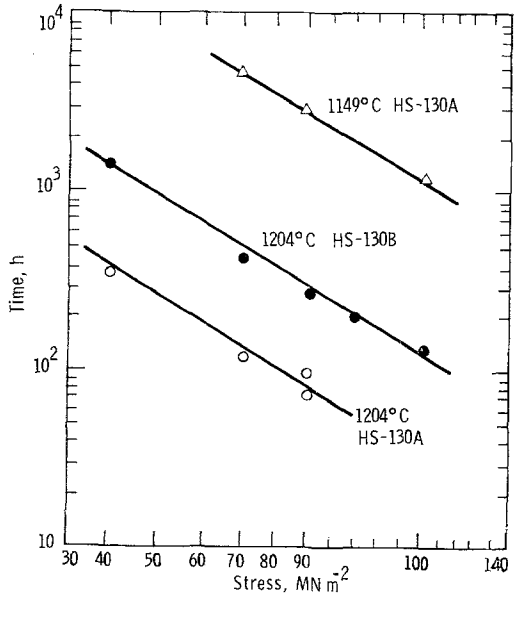

Figure 7 Time to 1% creep strain as a function of stress, in air.

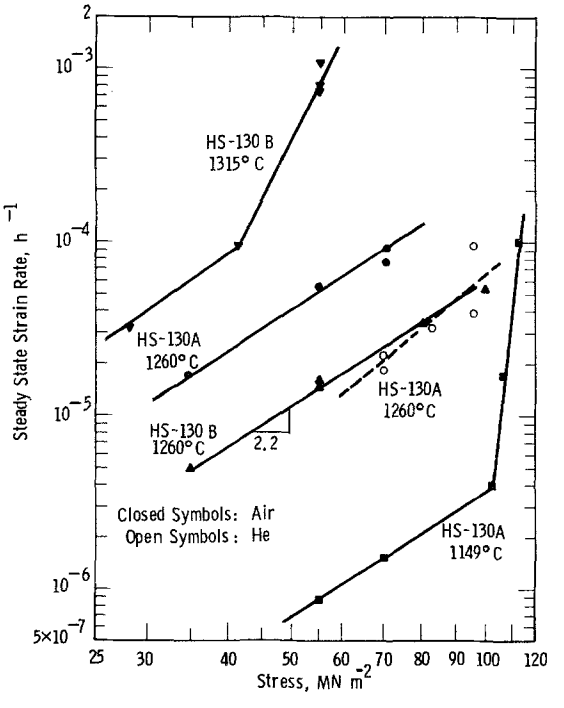

Figure 8 Steady state creep rate versus stress.

TABLE II Summary of creep tests, hot-pressed Si_3N_4

Specimen no.	Chemistry group	Test temperature (°C)	Atm	Stress σ, (MN m^{-2})	$\dot{\epsilon}_s$ (h^{-1})	Life t_{tr} (h)	Total strain ϵ (%)	Notes
1	HS-110 A	1204	air	55.1	—	1.5	0.6	1
2	HS-110 A	1204	air	55.1	—	0.3	0.4	1
3	HS-110 A	1204	air	41.3	1.5×10^{-3}	1.1	0.5	
4	HS-110 A	1204	air	27.6	1.0×10^{-5}	1063	2.2	2
5	HS-110 B	1149	He	103.0	—	0.3	0.15	
6	HS-110 B	1149	He	82.7	4.1×10^{-5}	0.9	0.23	
7	HS-110 B	1149	He	68.9	3.2×10^{-5}	0.6	0.26	
8	HS-110 B	1149	He	55.1	1.0×10^{-5}	439	1.07	
9	HS-130 A	1371	He	103.0	—	0.1	0.32	1
10	HS-130 A	1371	He	68.9	1.8×10^{-3}	2.4	0.71	
11	HS-130 A	1260	He	96.5	3.6×10^{-5}	42.7	0.49	
12	HS-130 A	1260	He	96.5	9.3×10^{-5}	17.2	0.55	
13	HS-130 A	1260	He	82.7	3.2×10^{-5}	86.8	0.39	
14	HS-130 A	1260	He	68.9	2.2×10^{-5}	130	0.47	
15	HS-130 A	1260	He	68.9	1.8×10^{-5}	600	1.28	
16	HS-130 B	1260	H3	68.9	4×10^{-5}	53	0.25	
17	HS-130 A	1204	He	82.7	1.7×10^{-5}	174	0.34	
18	HS-130 A	1318	He	68.9	—	0.3	—	1
19	HS-130 A	1288	He	68.9	6.5×10^{-3}	120	1.0	
20	HS-130 A	1260	air	68.9	1×10^{-4}	326	3.8	
21	HS-130 A	1260	air	68.9	7×10^{-5}	322	3.3	
22	HS-130 A	1260	air	55.1	6×10^{-5}	515	3.3	
23	HS-130 A	1260	air	34.5	1.8×10^{-5}	1252	2.7	
24	HS-130 B	1260	air	103.0	5.5×10^{-5}	384	3.0	
25	HS-130 B	1260	air	82.7	3.5×10^{-5}	736	3.4	
26	HS-130 B	1260	air	55.1	1.6×10^{-5}	1920	3.7	
27	HS-130 B	1260	air	34.5	5.0×10^{-6}			3
				55.1	1.4×10^{-5}			3
				68.9	2.9×10^{-5}			3
28	HS-130 B	1315	air	55.1	6.8×10^{-4}	51.7	3.8	
29	HS-130 B	1315	air	55.1	1.2×10^{-3}	18.6	2.4	
30	HS-130 B	1315	air	55.1	7.4×10^{-4}	11.4	1.4	4
31	HS-130 B	1315	air	41.4	9.8×10^{-5}	400	5.8	
32	HS-130 B	1315	air	27.6	3.2×10^{-5}	1064	5.5	
33	HS-130 A	1315	air	55.1	2.4×10^{-3}	2.8	1.0	5
34	HS-130 A	1315	air	68.9	1.1×10^{-2}	1.5	1.0	5
35	HS-130 A	1204	air	96.5	9×10^{-5}	67	1.0	
36	HS-130 A	1204	air	68.9	1.2×10^{-5}	1675	2.3	
37	HS-130 B	1204	air	82.7	4×10^{-6}			
38	HS-130 B	1204	air	110.2	1×10^{-3}	21.2	0.50	
39	HS-130 B	1149	air	103.0	4×10^{-6}	1000	0.85	2
40	HS-130 B	1149	air	68.9	1.5×10^{-6}	1097	0.55	2
41	HS-130 B	1149	air	55.1	8.5×10^{-7}	1000	0.42	2
42	HS-130 B	1092	He	68.9	3×10^{-6}			6
		1149	He	68.9	4×10^{-5}			6
		1180	He	68.9	1×10^{-4}			6
43	HS-130 A	1000	air	68.9	1.6×10^{-7}	1000	0.12	2

Notes:
1. Stage III creep only.
2. Test interrupted before failure.
3. Stress cycled.
4. Failed outside gauge section.
5. Fast transition to stage III.
6. Temperature cycled.

creep rate is plotted versus stress for various temperatures, levels of purity, and test environment. The data show that the steady state creep rate is related to stress through the power function $\dot{\epsilon}_s \propto \sigma^n$ where the exponent is about 2 between 1149 and 1200°C in air for the stress limits studied. While the best fit straight line for 1315°C data in air yield a stress exponent of 4.8, it seems more reasonable to acknowledge an abrupt change in slope when the stress level reaches 40 MN m^{-2}. At 1260°C in helium, the stress exponent approaches 3 indicating an atmospheric effect.

Strain rate is plotted as a function of $1/T$ in Fig. 9. The activation enthalpy is dependent upon the test environment and material purity, i.e. ΔH_c is higher for tests conducted in helium than for tests conducted in air and ΔH_c decreases as impurities in the material increase. Actual values of activation enthalpy are 535, 630 and 546 kJ mol^{-1} for HS-130 A Si_3N_4 in air, HS-130 A Si_3N_4 in helium, and HS-110 B Si_3N_4 in helium, respectively.

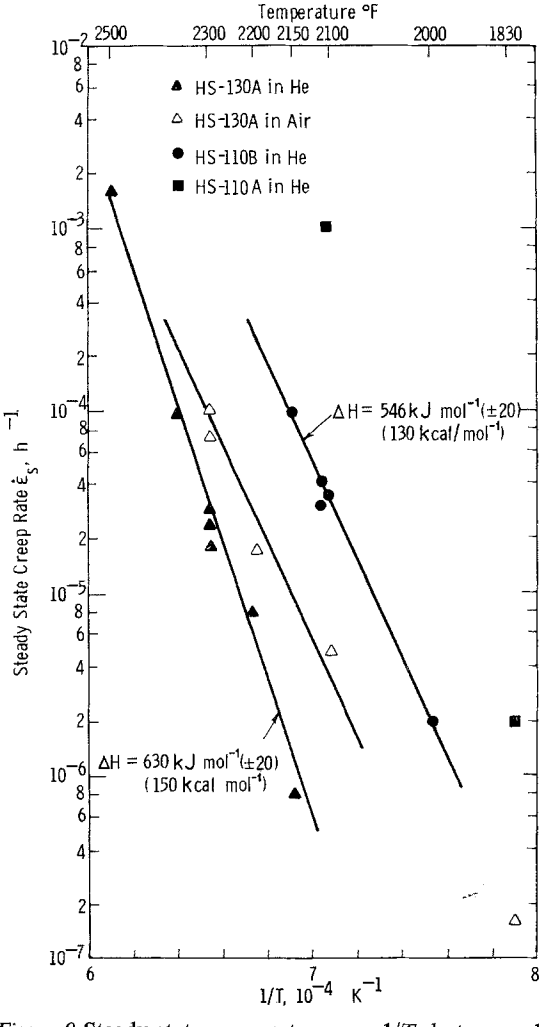

Figure 9 Steady state creep rate versus $1/T$; hot-pressed Si_3N_4 at 70.5 MN m^{-2}.

Temperature-compensated creep rate data corrected to 1200°C are used to demonstrate that the activation enthalpy for creep in Si_3N_4 depends upon stress. The data points in Fig. 10 were selected from tests conducted in air from purity groups HS-130A and HS-130B.

Figs. 8 to 10 indicate that both stress and temperature affect the creep rates as separate, independent functions of Equation 2, and that creep in Si_3N_4 is controlled by a single activated mechanism.

3.2. Results of microscopy

Low magnification micrographs of fracture surfaces from a tensile and a creep specimen are shown in Fig. 11a and b, respectively. The origin of fracture in the low temperature tensile test (Fig. 11a) is located at the centre of the flat semi-circle (arrow). This is a characteristic feature found on fractured surfaces of ceramic materials and is referred to as the "mirror" on the fracture surface. The appearance of the fracture surface of the creep specimen (Fig. 11b) is different from that of the tensile specimen. Here, the origin of fracture also occurs at the outer surface, but it is associated with a large area that appears rough.

A number of fracture surfaces from tensile and flexural test specimens were examined by replica transmission microscopy [6, 9]. Fracture surfaces similar to those shown in Fig. 11 appear in Fig. 12. The intergranular nature of room temperature fracture is evident in Fig. 12a. Intergranular fracture is the dominant failure mode at all test temperatures. The micrographs in Fig. 12b and c are typical of fracture in creep specimens.* Fig. 12c was taken from the rough surface associated with the origin of failure (surface B, Fig. 11b), while Fig. 12b represents the smooth part of the surface (A, Fig. 11b). Deep grain-boundary grooving and secondary intergranular cracking are evident in Fig. 12c, while Fig. 12b appears similar to the room temperature fracture shown in Fig. 12a.

*For clarity, the surface of a creep specimen tested in He is shown in Fig. 12. Although the fracture surfaces of specimens tested in air were covered with an oxide layer, the intergranular nature of the fractures could be recognized.

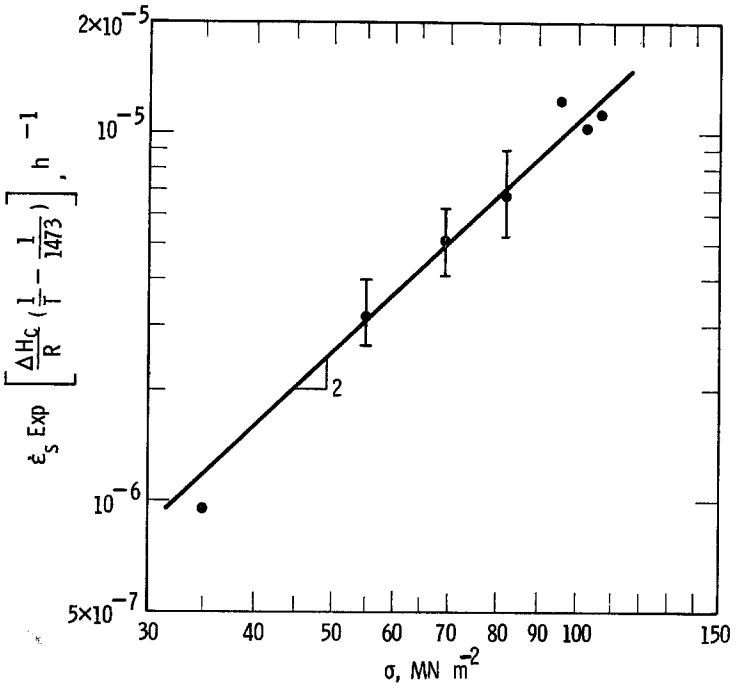

Figure 10 Temperature compensated steady creep rate versus stress tests between 1000 and 1200°C.

Transmission electron micrographs of foils prepared from a few creep specimens are shown in Fig. 13. In all cases, the foils represent areas less than 1 mm away from the fracture surface. The micrographs showing cavitation were taken from areas removed as far as possible from the edge of the foil to insure that the cavitation was not influenced by thinning artifacts [7].

The dominant features observed in transmission microscopy of creep specimens are (1) the extensive cavitation and (2) grain-boundary separation [6] (Fig. 13c). Occasional dislocation tangles (Fig. 13b) were observed, but these were no different in nature or frequency of occurence than the normal dislocation structures observed in hot-pressed Si_3N_4 [3, 10].

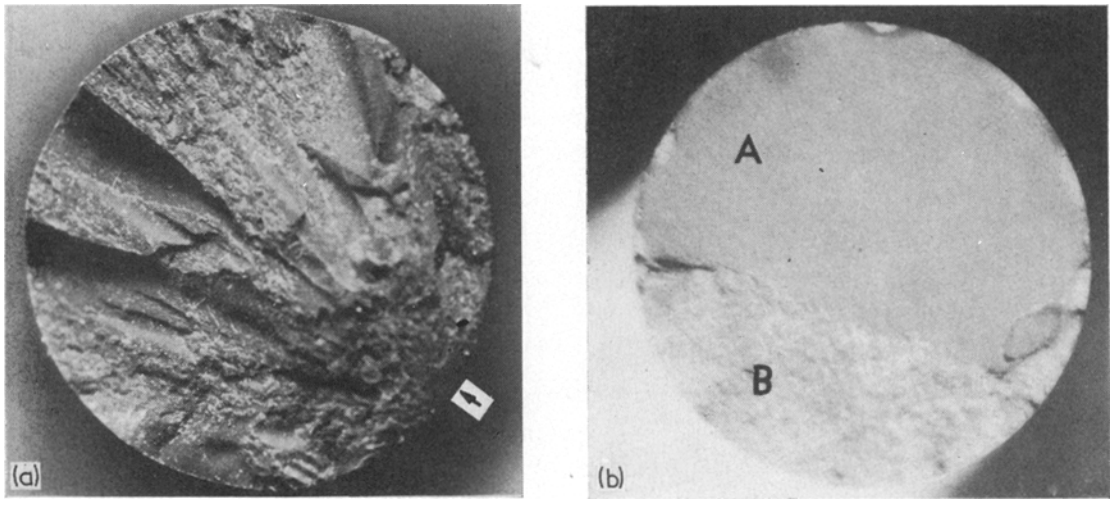

Figure 11 Light micrographs of fracture surface. (a) Tensile specimen, room temperature. "Mirror" fracture origin marked; (b) creep specimen, 1260°C in He. "Rough" surface of final crack growth at bottom, × 10.

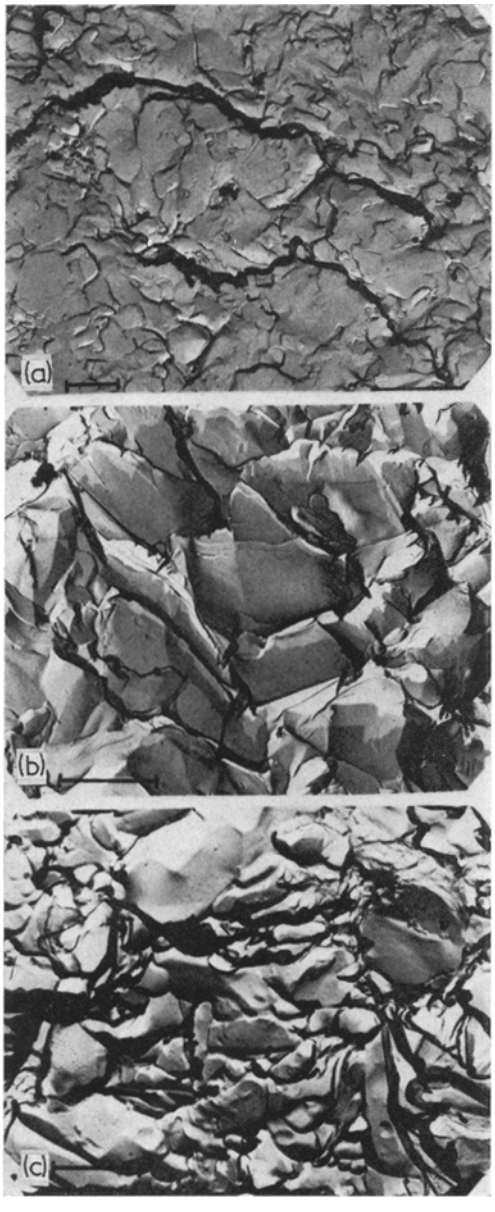

Figure 12 Replica transmission micrographs of fracture surfaces. (a) Tensile specimen, room temperature test; (b) creep specimen, 1260°C test, near centre of specimen; (c) same specimen as in (b) in rough area of fracture (Fig. 11b). Bars ≡ 1 μm.

4. Discussion

Evans and Sharp [10] and Kossowsky [3] have indicated that dislocation motion is not observed in Si_3N_4 and that it is not likely to occur at temperatures below 1700°C. It was also shown [5, 6] that even if dislocations were mobile at temperatures below 1400°C, their contribution to the total strain could not exceed 10^{-5}. The observed strains during creep of Si_3N_4 are of the order of 10^{-2}. The micrographs (Figs. 12 and 13) do not show evidence of deformation within the grain. All the micrographs indicate that deformation and failure during creep are a direct result of deformation and failure of the grain-boundary glass phase [11], which was identified as a silicate of magnesium containing Ca, Al, Na and K [3]. Therefore, deformation in hot-pressed Si_3N_4 should be explained in terms of, (1) the flow characteristics of the grain-boundary glass phase which bonds rigid, non-deformable grains together, and (2) the geometric constraints imposed by the system.

Certain impurities, particularly the alkaline oxides, have a profound effect on the softening point and viscosity of glass [12, 13]. Additions of 5 mol % CaO, for example, cause a sharp reduction in the softening point of SiO_2 and about two orders of magnitude decrease in the viscosity of the glass [13] at any given temperature. Since CaO is present in the grain boundaries of HS-130 Si_3N_4 in amounts approaching 12 mol % and since more than twice as much CaO has been found in the grain boundaries of the HS-110 material [3, 14], one would expect to find a significant difference in the creep strengths of these two grades of Si_3N_4. Indeed, the data in Table II and Figs. 6 to 9 indicate this to be the case and demonstrate the strong effect of alkaline impurities on the creep behaviour of Si_3N_4. These effects justify the classification of the various billets into four groups according to their chemistry (Table I).

The activation energy for diffusion of alkali and alkaline earth metals through glass vary between 84 kJ mol^{-1} (20 kcal mol^{-1}) and ~ 336 kJ mol^{-1} (80 kcal mol^{-1}) [15]. Since the activation enthalpy for creep in Si_3N_4 is much higher (630 kJ mol^{-1}), the diffusion of alkaline impurities must be eliminated as a rate controlling process. The ΔH_c obtained and the effect of impurities on ΔH_c (Fig. 9) are rather in agreement with the activation of viscous flow of silicate glasses (600 kJ mol^{-1}) [13]. We conclude, therefore, that creep deformation in Si_3N_4 is governed, apparently, by the viscous flow of the grain-boundary glass phase where strain is generated through a process of grain-boundary sliding.

Zener ([16], p.3) and Cottrell [17] showed that wedge cracks have to open at the grain

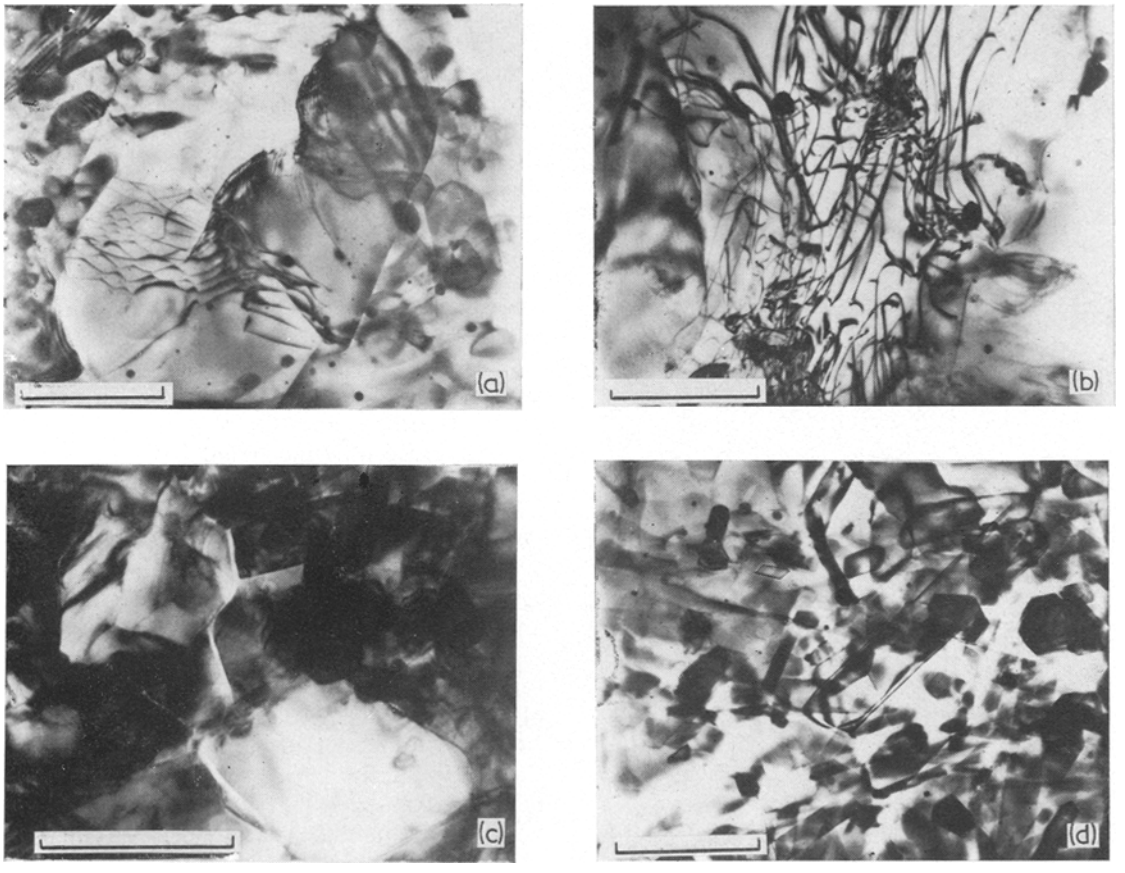

Figure 13 Transmission electron micrographs of creep specimen. (a) Dislocation network, 1149°C, 70.5 MN m^{-2}; (b) dislocation tangles, 1149°C, 82.7 MN m^{-2}; (c) grain-boundary separations, 1260°C, 70.5 MN m^{-2}; (d) extensive cavitation, 1260°C, 82.7 MN m^{-2}. Bars ≡ 1 μm.

junctions in order to maintain strain continuity during non-accommodated grain-boundary sliding. The model for creep deformation in Si_3N_4 is illustrated in Fig. 14. The initial stage or the transition stage is characterized by the successive nucleation of triple-point wedges as deformation spreads through the gauge section. During steady state creep or stage II (Fig. 14b), the wedges are assumed to grow at a rate which is proportional to the creep rate. An expression for the growth rate of the wedge cracks was obtained by Williams [18]:

$$\frac{dc}{dt} \approx \frac{\mu\sigma D^2\dot{\epsilon}_s^2 t}{4\pi(1-\nu)} \quad (3)$$

where μ is the shear modulus, σ is the stress, D is the average grain size, t is time, and $\dot{\epsilon}_s$ is the steady state creep rate. Note here that temperature is not included in the Equation 3 directly since the growth rate depends only on the relationship between stress and strain rate. When strain reaches a limiting value, grain-boundary separations link to form unstable cracks which continue to grow (Fig. 14c). This marks the onset of accelerated or stage III creep. It is essential to realize that the growth of the triple-point wedge cracks is geometrically necessary and occurs only as a direct consequence of creep deformation by grain-boundary sliding. The rate of crack propagation in stage III, however, is dependent upon stress rather than the rate of grain-boundary sliding. At this stage, the growth kinetics of the crack can be better described by fracture mechanics principles.

Williams derived an expression for the rate dependence of the time-to-failure on grain size and steady state creep rate from Equation 3:

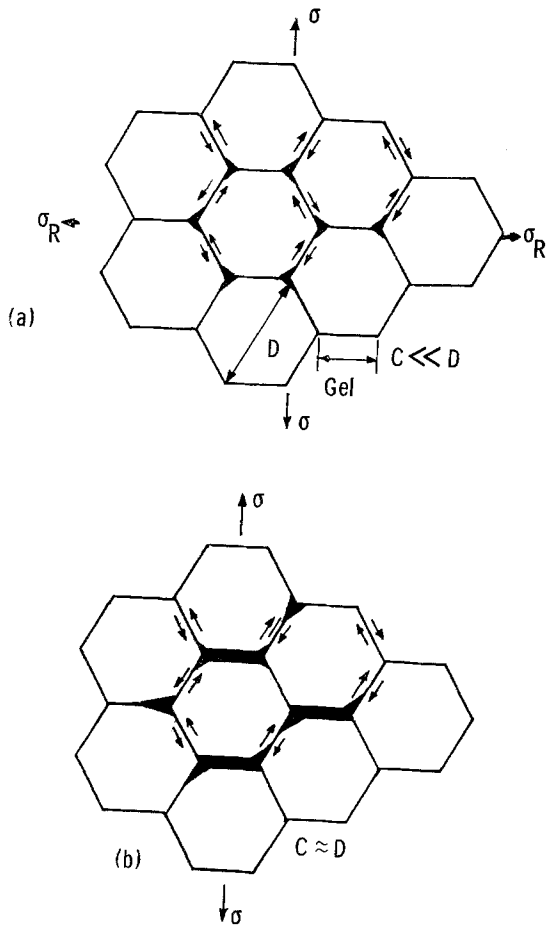

Figure 14 Schematic drawings of progressive, non-accommodating deformation by grain-boundary sliding. (a) Initial stage (end of stage I in creep), geometrically necessary. (b) Advanced stage. Grain-boundary cracks (stage II in creep). (c) Macroscopic crack motion (stage III in creep), energetically necessary.

$$t_{fr} = \left[\frac{G_{EL}8\pi(1-\nu)\gamma}{\mu D^2}\right]^{1/2} \dot{\epsilon}_s^{-1} \qquad (4)$$

where G_{EL} is the grain edge length, γ is the fracture energy, and the other symbols are as before. Equation 4 implies that, for given grain size and temperature, $t_{fr} \cdot \dot{\epsilon}_s$ is a constant which is independent of stress and equal to the total strain.

For conditions where $G_{EL} = 5 \times 10^{-5}$ cm, $D = 1.5 \times 10^{-4}$ cm, $\gamma = 1.25 \times 10^{12}$ dyn cm^{-2};

$$t_{fr}(h) \approx 3.2 \times 10^{-2}\, \dot{\epsilon}_s^{-1}. \qquad (5)$$

t_{fr} versus $\dot{\epsilon}_s$ is plotted for four different temperatures and five stress levels ranging from 55.1 to 103 MN m^{-2} (Table II) in Fig. 15. An intercept of 2.9×10^{-2}, measured for tests in air, compares well with Equation 5. In plotting the data in Fig. 15, variations in γ and μ were ignored within the range of the test temperatures.

The solid line in Fig. 15 and Equation 5 thus indicates that Si_3N_4 is creep-strain limited in an air environment. The data also indicate that the general creep mechanism operates for tests in an He atmosphere. Total strains, however, are much lower (Fig. 15) and the dispersion of the data around the dashed line is rather high.

Failure in creep always originates from the external surface (Fig. 11). This may be due to an incremental difference in stress at the surface resulting from minor misalignment. Furthermore, critical cracks which determine final failure (Fig. 14c) are probably larger at the external surface than critical cracks occurring internally. Consequently, pre-existing cracks will cause the creep behaviour to deviate from that predicted by Equation 4, i.e. reduced stress rupture life. However, if surface imperfections are neutralized, creep deformation can proceed according to the theoretical predictions.

The rapid formation of a Ca-rich silicate, as an oxidation product on the surface of Si_3N_4 exposed to elevated temperature in air, was observed by Singhal [19]. Dissolution of Si_3N_4 in silicate glasses was also reported [20]. Therefore, exposure to air can provide a fast and effective mechanism to smooth surface imperfections and "heal" crack type defects. This may account for the differences in creep strain at failure for specimen tested in air and in helium,

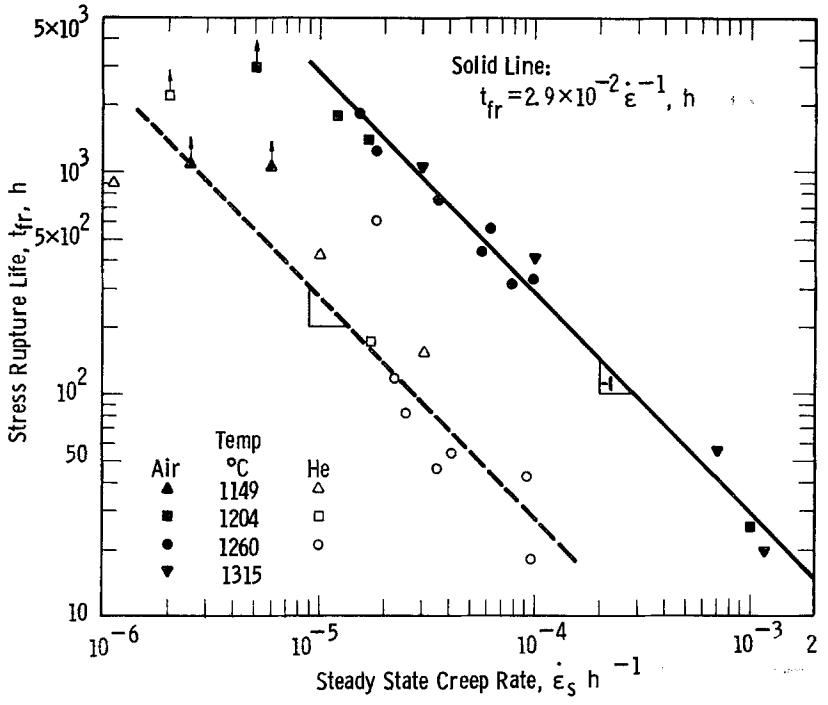

Figure 15 Dependence of stress rupture life on creep rate, hot-pressed Si_3N_4.

but it does not explain differences in creep rate satisfactorily.

The nucleation and growth of wedge cracks decrease the effective area supporting the load. Consequently, the void-containing areas will experience higher stress which will induce an increase in the creep rate. It follows that the effective stress, controlling grain-boundary sliding, is higher than the apparent stress in a body. Deviations from pure Newtonian viscosity will be manifested in strain rate versus applied stress relations where the exponent n (Equation 2) is greater than 1. At high stresses, or temperatures, n may deviate far from unity as indicated by the creep data at 1315°C (Fig. 8). Similar observations were reported recently by Morrell and Ashbee [21] in their study of creep behaviour in glass ceramic systems. Although the deformation process was rate controlled by the viscous flow of a residual glass phase, void formation during creep modified the rate dependence of stress beyond that expected from a simple Newtonian flow. Only where the viscous glass is free to flow and fill the voids as they are formed will pure Newtonian creep ($n = 1$) prevail. Even then, two conditions must be met; (1) void formation must create a hydrostatic pressure gradient favouring viscous flow into the voids and (2) there must be sufficient glass available to fill the voids from the grain boundaries.

It may be possible to account for the observed differences in the creep rates of Si_3N_4 in air ($n = 2$) and helium ($n = 2.9$) in terms of the amount of glass phase present. Consider the case of creep in helium where the grain boundaries represent a capillary network completely filled with glass. As wedges open under static stress, the hydrostatic pressure gradient must exceed the surface tension before the glass can flow from the grain boundaries into the void (Fig. 16). In air, the volume of glass increases by the solution of oxidation products at the surface. As long as the capillary (grain boundary) is supplied with glass, flow will occur under the influence of the hydrostatic pressure gradient alone since surface tension will not prevent flow as long as surface oxidation provides a continuous source of glass.

The results of a microprobe analysis tend to support this hypothesis of glass flow in air. Creep specimens tested in air and helium are compared in Fig. 17. There is little evidence of alkali ion migration in the specimen tested in helium while potassium and to a lesser extent

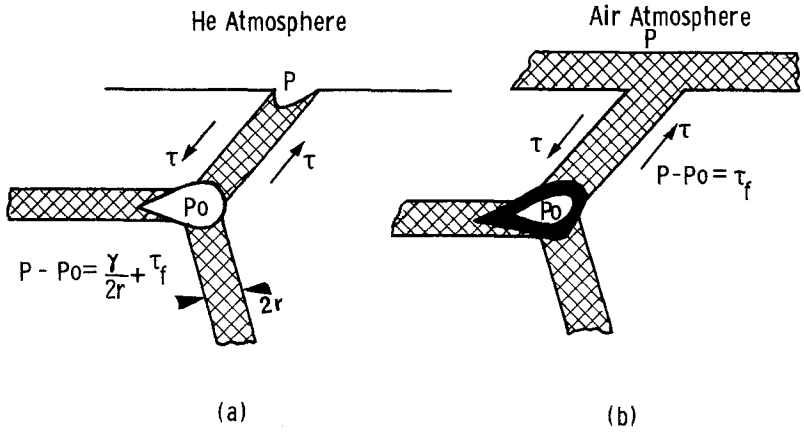

Figure 16 Model of glass flow through grain boundaries. (a) Effect of air environment versus helium. Increase in creep rate ($\dot{\epsilon}\uparrow$); increase in creep strain ($\downarrow\uparrow$); decrease in activation energy ($\Delta H_c\epsilon$). (b) Effect of alkaline impurities. Increase in creep rate ($\dot{\epsilon}\uparrow$); increase in creep strain ($\dot{\epsilon}\uparrow$); decrease in activation energy ($\Delta H_c\downarrow$).

sodium migration from the glass filled void is apparent in the specimen tested in air. The glass filled voids are characteristic of Si_3N_4 microstructure. Microprobe scans of void areas in the as-received material closely resemble these taken from specimens tested in helium.

The creep strength in compression should be higher than the creep strength in tension as another consequence of grain-boundary sliding which involves rigid, non-deformable grain [21]. Here, strain in the direction of the applied load is accommodated by compression of the boundary glass phase, while lateral motion (bulging) results from stresses resolved in a direction perpendicular to the applied load (σ_R, Fig. 14a). A specimen tested in compression at 1370°C in air had to be loaded to 689 MN m^{-2} to produce a steady state creep rate of 5.5×10^{-4} h^{-1}. This is more than 10 times the stress required to produce a similar creep rate in the tensile mode.

Finally, since the grain-boundary glass phase controls the stress-strain behaviour of hot-pressed Si_3N_4, the elastic modulus should be rate dependent and that rate dependence should be temperature dependent. Zener ([16], p. 44) showed that the elastic modulus in an "unelastic" solid such as hot-pressed Si_3N_4 has two values, M_R and M_u, the relaxed and unrelaxed modulus, respectively. M_u dominates at a high rate of loading, while M_R dominates during slow rate of loading where relaxation can take place. M_R and M_u are related through the expression:

$$\frac{M_u}{M_R} = \frac{\tau_\sigma}{\tau_\epsilon} \quad (7)$$

where τ_σ is the stress relaxation time under constant strain and τ_ϵ is the strain relaxation time under constant stress. At low temperature, $\tau_\sigma/\tau_\epsilon \approx 1$ and thus $M_u \approx M_R$. This is confirmed by Fig. 4 which shows that at room temperature there is a close agreement between the elastic modulus measured by sonic resonance and elastic modulus measured from uniaxial tensile tests at a loading rate of 1×10^{-3} min^{-1}. At high temperature where relaxation takes place, M_u/M_R becomes larger than unity because the frequency and temperature dependence of the ratio is related to the internal friction characteristics of the material ([16], p. 44). Therefore, as temperature is increased beyond room temperature, the moduli obtained from tensile specimens will decrease at a higher rate than the modulii obtained from sonic resonance measurements (Fig. 4).

5. Summary and conclusions

The high temperature strength of Norton HS-110 and HS-130 hot-pressed Si_3N_4 is controlled by grain-boundary glass phase which bonds hard, non-deformable grains. Consequently, it was shown that:

(1) Deformation occurs by the mechanism of grain-boundary sliding;

(2) Temperature and impurities, such as Ca, control the creep behaviour of the material through their effect on the viscous flow of the grain-boundary glass phase. Lowering the amount of Ca present to below 100 ppm should greatly improve creep strength;

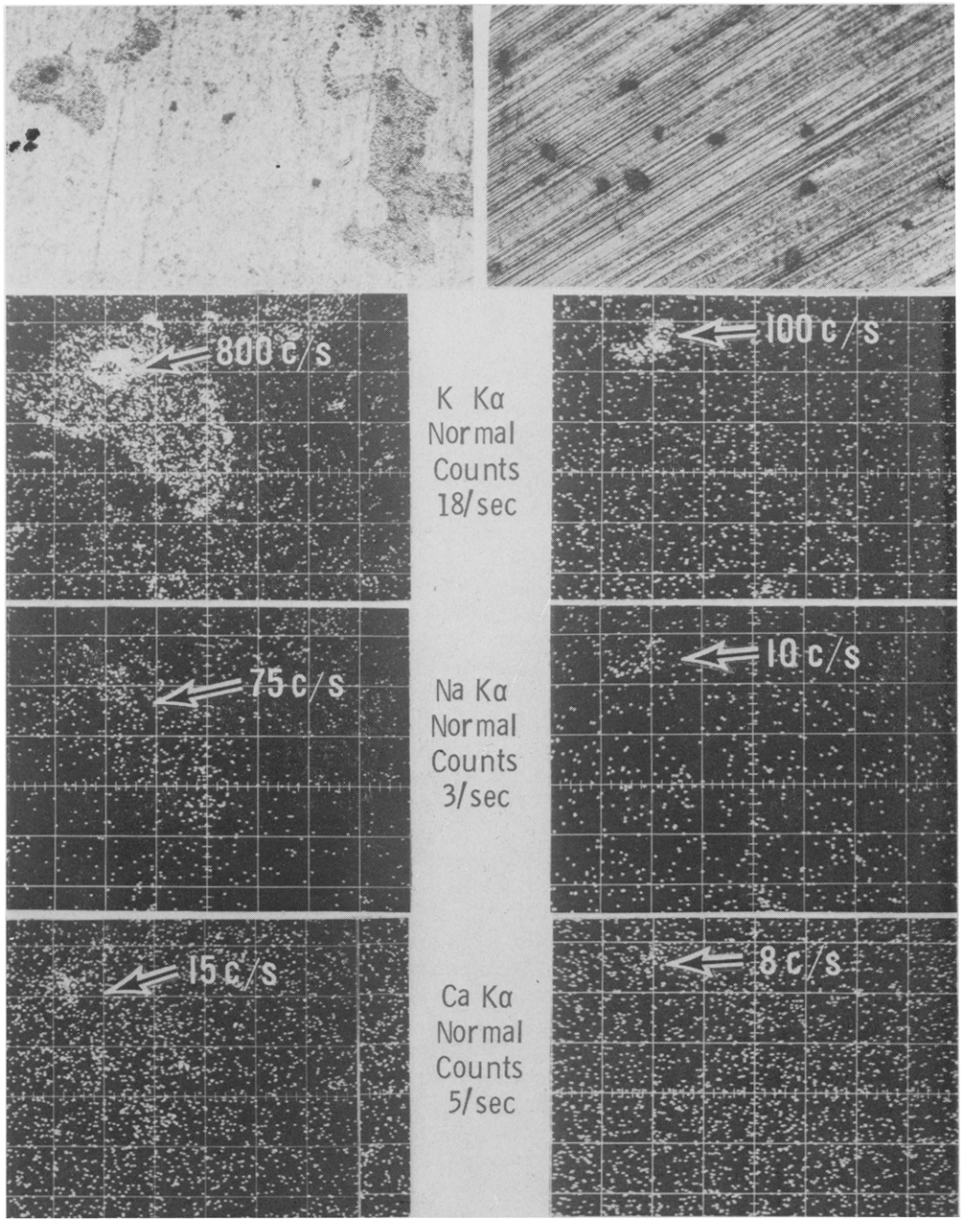

Figure 17 Alkaline distribution in Si_3N_4 specimen after creep. Top row: light micrographs, × 100; Below, microprobe traces. Left column: creep test in air. Right column: creep test in He, both at 1260°C × 225.

(3) Hot-pressed Si_3N_4 is creep strain limited under most of temperature and stress conditions investigated;

(4) As a consequence of creep deformation, wedge cracks open at the grain junctions. The growth of these cracks is a geometrical necessity with the rate of growth of these cracks being related proportional to the creep rate;

(5) Wedge cracks eventually coalesce to terminate the stage of steady state creep and

rapidly lead to a final failure of the material.

Acknowledgements

This work was supported by the Advanced Research Projects Agency, Contract DAAG-44-71-C-0162. Technical assistance was provided by T. J. Mullen and C. M. Fox. Many of the He tests were conducted at the Westinghouse Astronuclear Laboratories by G. Yatsko.

References

1. E. GLENNY and T. A. TAYLOR, *Powder Met.* **48** (1961) 164; **44** (1958) 189.
2. A. F. MCLEAN, E. A. FISHER and R. J. BRATTON, AMMRC-CTR 72-3, 72-79, 73-9, 73-32 and 74-26, 1972-1974.
3. RAM KOSSOWSKY, *J. Mater. Sci.* **8** (1973) 1603.
4. DAVID N. RICHERSON, *Bull. Amer. Ceram. Soc.* **52** (1973) 560.
5. RAM KOSSOWSKY, *J. Amer. Ceram. Soc.* **56** (1973) 531.
6. RAM KOSSOWSKY, in "Ceramics for High Performance Applications", (Brook Hill, 1974).
7. RAM KOSSOWSKY and G. P. SABOL, in "Specimen Preparation Techniques for Electron Microscopy", edited by J. L. McCall and W. M. Mueller, (Plenum Press, New York, 1974) p. 333.
8. Fifth Semi-Annual Report, ARPA Contract DAAG 44-71-C-0162, March 1974.
9. RAM KOSSOWSKY and W. C. FRAZIER, paper presented at the 75th Annual Meeting, American Ceramic Society, Cincinnatti, May 1973.
10. A. G. EVANS and J. V. SHARP, *J. Mater. Sci.* **6** (1971) 1292.
11. S. WILD, P. GRIEVESON and K. H. JACK, in "Special Ceramics", Vol. 5, edited by P. Popper (British Ceramic Research Association, 1972) p. 377.
12. W. D. KINGERY, "Introduction to Ceramics" (Wiley, New York, 1966).
13. R. ROSEN, J. BERSAN and G. URBAIN, Rev. Houtes Temp. Bt. Refract. (in French) **1** (1964) 159.
14. RAM KOSSOWSKY and S. C. SINGHAL, in "Grain Boundaries in Engineering Materials", Fourth Bolton Landing Conference, to be published.
15. PERRIN WINCHELL, *High Temp. Sci.* **1** (1969) 200.
16. C. ZENER, "Elasticity and Unelasticity", (University of Chicago Press, 1948) p. 3.
17. A. H. COTTRELL, "Structural Processes in Creep", (Iron and Steel Institute, London, 1961).
18. J. A. WILLIAMS, *Phil. Mag.* **20** (1968) 1289.
19. S. C. SINGHAL, paper presented at the 75th Annua Meeting, American Ceramic Society, Cincinnatti, May 1973.
20. RAM KOSSOWSKY, *J. Mater. Sci.* **9** (1974) 2025.
21. R. MORRELL and K. H. G. ASHBEE, *ibid* **8** (1973) 1253.

Received 16 October and accepted 28 November 1974.